- Data-Driven Materials Discovery of Oxygen-Rich Hyperporous Carbons
- 2 for Carbon-Based Supercapacitors
- 3 Tao Wang, 1,2 Musen Zhou, 3 Murillo L. Martins, 4 Runtong Pan, 3 Jinlei Cui, 5 Zhennan Huang, 6
- 4 Bishnu P. Thapaliya, 1,2 Chi-Linh Do-Thanh, 2 Juntian Fan, 2 Zhenzhen Yang, 1,2 Miaofang Chi, 6
- 5 Takeshi Kobayashi, <sup>5</sup> Jianzhong Wu, <sup>3</sup> Eugene Mamontov, <sup>4</sup> Sheng Dai<sup>1,2\*</sup>
- 6 <sup>1</sup> Chemical Sciences Division, Oak Ridge National Laboratory, Oak Ridge, TN 37831, USA
- 8 Tennessee, Knoxville, Tennessee 37996, USA
- 9 <sup>3</sup> Department of Chemical and Environmental Engineering, University of California, Riverside,
- 10 Riverside, California 92521, USA
- <sup>4</sup> Neutron Scattering Division, Oak Ridge National Laboratory, Oak Ridge, Tennessee 37831, USA
- 12 5 U.S. DOE Ames Laboratory, Ames, Iowa 50011, USA
- 13 <sup>6</sup> Center for Nanophase Materials Sciences, Oak Ridge National Laboratory. Oak Ridge,
- 14 Tennessee 37831, USA
- \*Email: dais@ornl.gov

#### 19 Methods

- 20 **Preparation of HCP-Ben.** 9.75 g of anhydrous ferric chloride was added to a solution of
- benzene (1.56 g) and FDA (4.56g) in 20 mL of 1,2-dichloroethane under stirring. The mixture
- was heated to 45  $^{\circ}$ C for 5 h and then to 80  $^{\circ}$ C for 19 h. The product was collected and washed with
- 23 methanol by vacuum filtration, and then washed with refluxed methanol in a Soxhlet extractor
- for 24 h. Then the product was dried at 60 °C in a vacuum oven.
- 25 **Preparation of HCP-Phe.** 6.50 g of anhydrous ferric chloride was added to a solution of phenol
- 26 (1.98 g) and FDA (3.04 g) in 20 mL of 1,2-dichloroethane under stirring. The mixture was
- heated to 45  $^{\circ C}$  for 5 h and then to 80  $^{\circ C}$  for 19 h. The product was collected and washed with
- 28 methanol by vacuum filtration, and then washed with refluxed methanol in a Soxhlet extractor
- 29 for 24 h. Then the product was dried at 60 °C in a vacuum oven.
- 30 **Preparation of HCP-Res.** 6.50 g of anhydrous ferric chloride was added to a solution of
- resorcinol (2.00 g) and FDA (3.04 g) in 20 mL of 1,2-dichloroethane under stirring. The mixture
- was heated to 45  $^{\circ}$ C for 5 h and then to 80  $^{\circ}$ C for 19 h. The product was collected and washed with
- methanol by vacuum filtration, and then washed with refluxed methanol in a Soxhlet extractor
- for 24 h. Then the product was dried at  $60^{\circ C}$  in a vacuum oven.
- 35 **Preparation of HCP-Phl.** 6.50 g of anhydrous ferric chloride was added to a solution of
- phloroglucinol (2.00 g) and FDA (3.04 g) in 20 mL of 1,2-dichloroethane under stirring. The
- 37 mixture was heated to 45  $^{\circ C}$  for 5 h and then to 80  $^{\circ C}$  for 19 h. The product was collected and
- washed with methanol by vacuum filtration, and then washed with refluxed methanol in a
- 39 Soxhlet extractor for 24 h. Then the product was dried at  $60^{\circ C}$  in a vacuum oven.

- 40 **Preparation of hyperporous carbons.** Taking the synthesis of C-Phl as an example, 0.50 g of
- 41 HCP was mixed with 1.00 g of NaNH<sub>2</sub> by hand grinding in an argon glove box. The mixture was
- heated to 350 °C for 1 hour with a heating rate of 5 °C/min and then to 600 °C for 2 hours with a
- heating rate of 5 °C/min in a tube furnace. After cooling to room temperature, the carbon product
- was washed with water and collected by vacuum filtration. Then the product was soaked in 3 M
- 45 HCl solution, heated to 60 °C for 5 hours, and washed with water again by vacuum filtration.
- 46 Finally, the product was dried at 100  $^{\circ}$ C in a vacuum oven to obtain the C-Phl. Other hyperporous
- 47 carbons were synthesized using their corresponding HCPs under the same condition.
- 48 C-Phl-700 and C-Phl-500 were synthesized by changing the heating temperature from
- 49  $600^{\circ C}$  to 700 and 500  $^{\circ C}$ , respectively. All the other treatments were the same as C-Phl.

## **Characterization techniques**

50

61

- 51 The X-ray diffraction (XRD) patterns were collected on a PANalytical Empyrean diffractometer
- with Cu Ka radiation, operated at 45 kV and 40 mA. X-ray photoelectron spectroscopy (XPS)
- was performed on a PHI 3056 spectrometer equipped with an Al anode source operated at 15 KV
- and an applied power of 350 W and a pass energy of 93.5 eV. Raman spectroscopy was
- performed on a Renishaw inVia confocal Raman microscope with a 532 nm laser. N<sub>2</sub> adsorption-
- desorption experiments were performed on a 3 Flex Micromeritics Setup at 77 K. 13C{<sup>1</sup>H}
- 57 crosspolarization magic-angle spinning (CPMAS) experiment was performed on a Bruker
- Biospin AVANCE I spectrometer, operated at 9.4 T equipped with a 4 mm double-resonance
- 59 MAS probe. A MAS rate of 7.5 kHz was used. STEM imaging was performed on probe-
- 60 corrected JOEL NEOARM electron microscope at 80 kV.

### Electrode preparation and electrochemical protocol

14 mg of hyperporous carbon, 4 mg of carbon black (acetylene black), 40 µl of Nafion solution 62 (5 wt%), and 0.96 ml of isopropanol were mixed to obtain an ink. 10 μl of the ink was drop cast 63 onto a polished glassy carbon rod as the working electrode. The mass loading of hyperporous 64 carbon on the working electrode was about 0.7 mg cm<sup>-2</sup>. Hg/Hg<sub>2</sub>SO<sub>4</sub> electrode (0.64 V vs NHE) 65 filling with a concentrated K<sub>2</sub>SO<sub>4</sub> supporting solution was used as the reference electrode, 1 M 66 H<sub>2</sub>SO<sub>4</sub> aqueous solution as electrolyte, and a piece of platinum mesh as the counter electrode. 67 The electrochemical data was collected on a CHI 760E instrument. The working electrode was 68 initially aged by cyclic voltammetry for 200 cycles at 100 mV/s, between -0.6 and 0.4 V vs 69 70 Hg/Hg<sub>2</sub>SO<sub>4</sub> to establish a stable cycling behavior. Then, cyclic voltammetry was performed at a series of scan rate from 1 to 500 mV/s between -0.6 and 0.4 V vs Hg/Hg<sub>2</sub>SO<sub>4</sub>. The average 71 capacitances were calculated from their CV data according to Eq. S1: 72

$$73 C = \frac{\int i_m E dE}{2v\Delta E} (S1)$$

- where C (F/g) is the specific capacitance, i<sub>m</sub> (A/g) and E (V) are specific current and potential in voltammogram, v (V/s) is the scan rate, ΔE (V) is the potential window.
- GCD tests were performed at a series of current densities from 0.2 to 100 A/g between -0.6 and 0.4 V vs Hg/Hg<sub>2</sub>SO<sub>4</sub>. SPECS measurements were performed using a potential step of 25 mV between -0.6 and 0.4 V with an equilibration time of 300 s.

# Machine learning models and methodology

79

80

81

82

83

In this work, artificial neural network (ANN) model is used predict the performance of N/O codoped activated carbon electrode in supercapacitor. The structural features used in ANN include micropore surface area ( $S_{micro}$ ) and mesopore surface area ( $S_{meso}$ ), while the total percentage of nitrogen and oxygen doping is used as the chemical features. In addition, scan rate is also used to

capture the decrease of capacitance at a faster charging/discharging rate. In the training database, electrochemical performance of N/O co-doped activated carbon electrode are collected in both 6M KOH and 1M H<sub>2</sub>SO<sub>4</sub> electrolyte. In the ANN model, the type of electrolyte is treated as dummy variable.

Based on literature data, ANN predicts the maximum capacitance of N/O co-doped activated carbon electrode in 1M H<sub>2</sub>SO<sub>4</sub> can be achieved with the micropore surface area of 3900 m<sup>2</sup>/g, mesopore surface area of 1000 m<sup>2</sup>/g, nitrogen-doping of 1 at% and oxygen-doping of 15 at%. Figure 1 shows the predicted capacitance and retention versus scan rate for the best N/O co-doped activated carbon electrode. According to the ANN prediction, in 1M H<sub>2</sub>SO<sub>4</sub> electrolyte, excess oxygen-doping would lead to significant increase of capacitance due to the increase of electronic conductivity and surface wetting.

### Description of the QENS samples and experimental details

For these experiments, the highly porous carbons defined in the main manuscript as C-Phl and C-Phl-700 have been investigated. The carbons were soaked overnight in 1M H<sub>2</sub>SO<sub>4</sub> solution and separated by fast vacuum filtration to remove free and loosely bound water. The final samples were defined as wet samples and had molar fractions of carbon of around 20% and 13% in C-Phl and C-Phl-700 respectively. Samples of dry carbon, that is, not soaked in the electrolyte, were also prepared and dried at 140 °C under vacuum for 72h.

The QENS experiments were performed at the BASIS spectrometer, which provides an energy resolution of 3.7  $\mu eV$  (full-width at half-maximum for the *Q*-averaged resolution value) and an accessible dynamical range of  $\pm$  100  $\mu eV$ . For the experiments,  $\sim$  40mg of the wet samples were placed in Au-coated Al flat plates, and sealed with indium gaskets. For the dry samples,  $\sim$ 

200 mg of each material was placed in Al flat plates and also sealed with indium gaskets. All these procedures were conducted in an Ar-filled glovebox.

The samples were initially cooled down to 20 K, and full QENS spectra were collected to be used as the instrumental resolutions. Then, temperature-dependent elastic scattering intensity scans were collected between 20 K and 300 K with 1K steps, and full QENS spectra were collected at 300 K. For background subtraction, data from empty sample holders (both Au-coated and not Au-coated) were collected at 300 K.

### **QENS** Results

In Figure S5a, the elastic scattering intensity scans summed over  $Q = 0.3-1.1 \text{Å}^{-1}$  are presented for the dry samples and the wet samples. In the figure, the data have been normalized by the mass of the samples. For the dry carbons, the monotonical behavior of the curves indicates that all the scattering species in these materials are either immobilized or perform motions that are not within the instrumental resolution. Here, the very slight decrease in intensity of the elastic scattering as the temperature increases is solely related to the Debye-Waller factor, and the very similar absolute intensities in both the dry samples indicate that these have very comparable numbers of H-rich species. For the wet samples, the higher scattering intensities as caused by the presence of the electrolyte can be contemplated. In Figure S5b, the data from the wet samples are reproduced with the datapoint at T = 20 K normalized to unity to allow for the observation of the temperature-dependent changes in the fraction of elastic scattering. In Figure S5c, the Q-dependence of the fractions of the elastic scattering intensities in the QENS signals at 300 K is presented and provides information about the portion of the material that does not perform detectable motions, as depicted by the data points at the highest Q-values. As expected, based on

the above-described synthesis of the materials and the respective final fractions of carbon in each sample, C-Phl-700 presents a lower percent of elastic scattering, 12%, than C-Phl, 20%.

Turning to the QENS spectra collected at 300K, these are presented in Figure 5b at Q = 0.7 Å<sup>-1</sup>. In Figure 5b, the QENS spectra are presented as the imaginary part of the dynamical susceptibilities, obtained via the following expression:

133 
$$\chi''(Q,E) \propto \frac{S(Q,E)}{n_B(T,E)} = S(Q,E) * \left[ exp\left(\frac{E}{kT}\right) - 1 \right]$$
 (S2)

where  $n_B(T, E)$  is the temperature Bose factor, k is the Boltzmann constant, T is the temperature, and S(Q, E) is the dynamic scattering function. For the presentation in Figure S6a, the signals from the dry samples could also be subtracted from the data from the wet materials to mitigate the influences of elastic scattering at the lowest frequencies. This test has been made and a similar outcome was obtained. With the presentation in Figure S6a, visual perception of two distinct components is possible in both samples. That is, relaxations above 10  $\mu$ eV are detected as well as a component around 1  $\mu$ eV. In the following lines, the origins of these components will be discussed and in Figures S6 b and c, their Q-dependences can be appreciated.

The component around 1  $\mu$ eV, which is visually different for C-Phl and C-Phl-700, is associated with the elastic scattering, hence with  $A_0(Q)$ . Indeed, if this component was associated not with elastic signal, but slow dynamics within the materials, as represented by  $\Gamma_N(Q)$  in equation (5), discrepancies in the p-factor, discussed in the main manuscript (see Figure 5d), between the two samples would be detected. Since this is not the case, the ca. 1  $\mu$ eV component must be elastic. Still, the presence of two dynamic processes is indicated by the two transitions in the elastic scattering intensity scans, displayed in Figure S5, and fitting S(Q, E) with a single component, either Lorentzian or a stretched function, does not lead to satisfactory

results. Therefore, we assume that the relaxation signal above 10  $\mu$ eV in Figure S6a is composed of a slower and a faster component, associated with  $\Gamma_N(Q)$  and  $\Gamma_B(Q)$  in Equation (5). If this supposition is valid, then the slope at the low-frequency side of the main relaxation must differ significantly from unity, indicating that the dynamic process under analysis does not consist of a single component. As shown in Figure S7, this is, indeed, the case (for completeness, the slopes at the high-frequency side are also shown).

# **Figures**

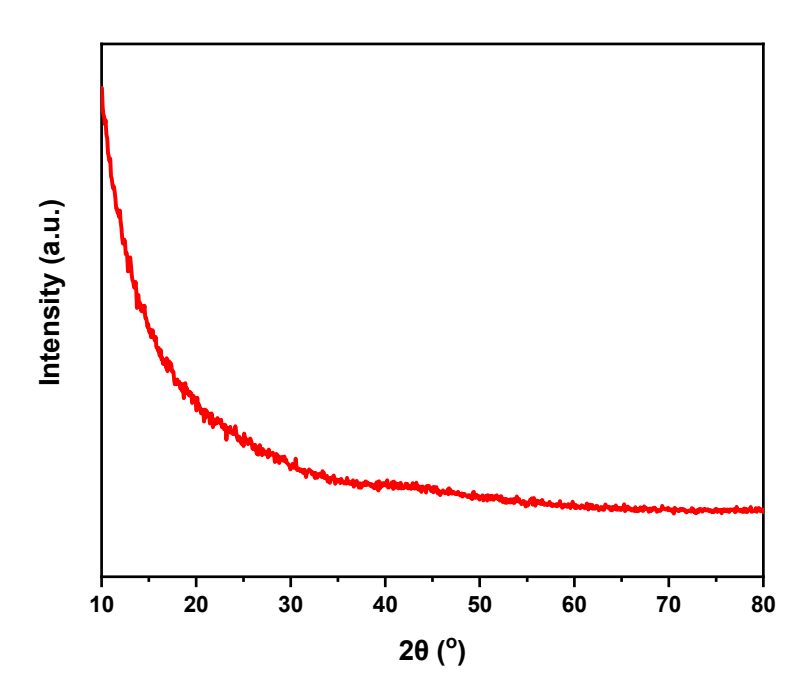
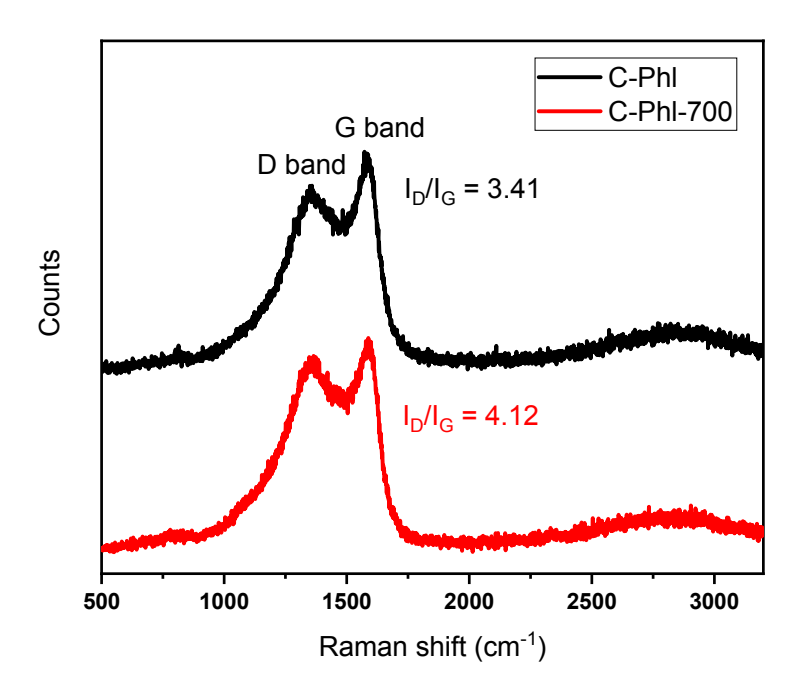


Fig. S1| Powder XRD pattern of C-Phl.



**Fig. S2**| **Raman spectra of C-Phl and C-Phl-700.** Raman spectra reveal the signals from the defects in graphitic lattice (D band) at 1353 cm<sup>-1</sup>, and the in-plane vibration of the sp<sup>2</sup> carbon network (G band) at 1590 cm<sup>-1</sup>. The high area ratio of D band to G band (I<sub>D</sub>/I<sub>G</sub>) above 3 indicates the amorphous nature of these carbon products.

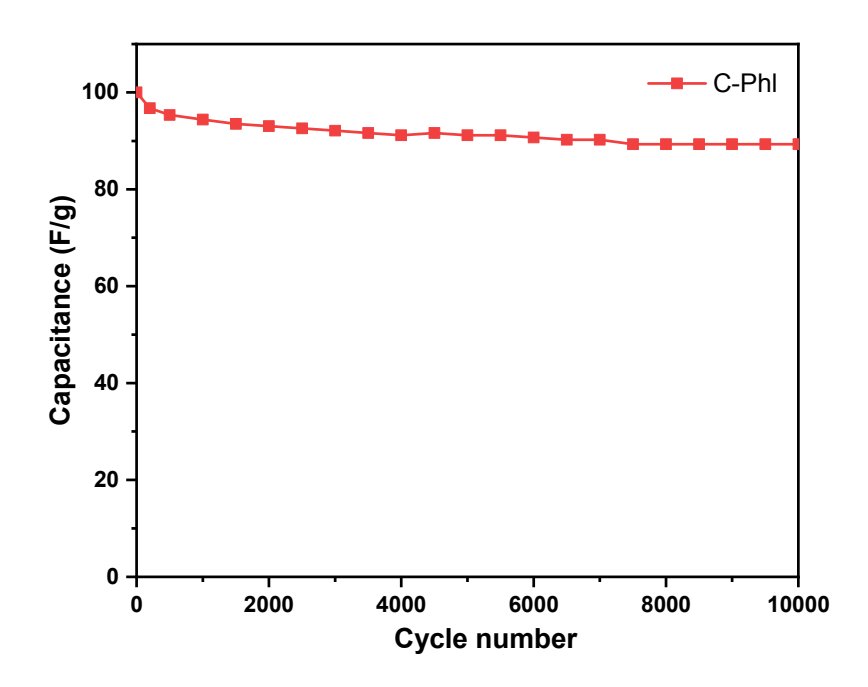


Fig. S3| Cycling performance of C-Phl at 20 A/g.

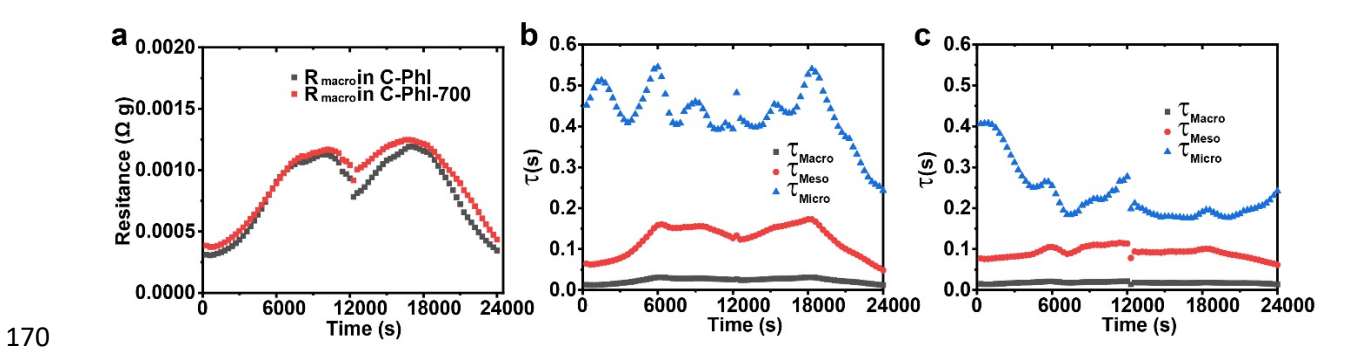


Fig. S4| Parameters fitted from the SPECS data of C-Phl and C-Phl-700. a) Macropore resistances; b) time constants of C-Phl; (c) time constants of C-Phl-700.

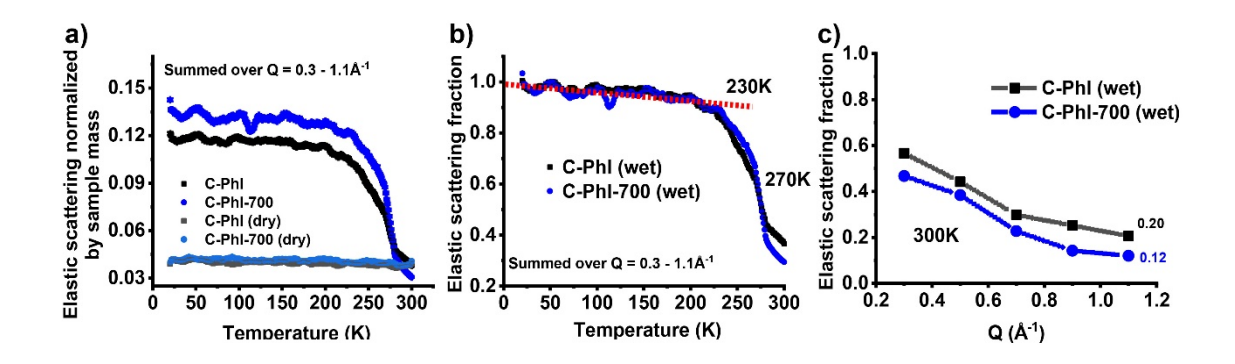


Fig. S5| Elastic scattering intensity scans (a) normalized by the samples' mass for the dry and wet samples, and (b) for the wet samples with the datapoints at T = 20 K normalized to unity. In both cases, the data are summed over Q = 0.3-1.1Å<sup>-1</sup>. In (c), the Q-dependences of the fraction of the elastic scattering intensities in the QENS signals at 300 K are presented. The numbers on the right-hand side indicate the elastic scattering fraction at Q = 1.1 Å<sup>-1</sup>.

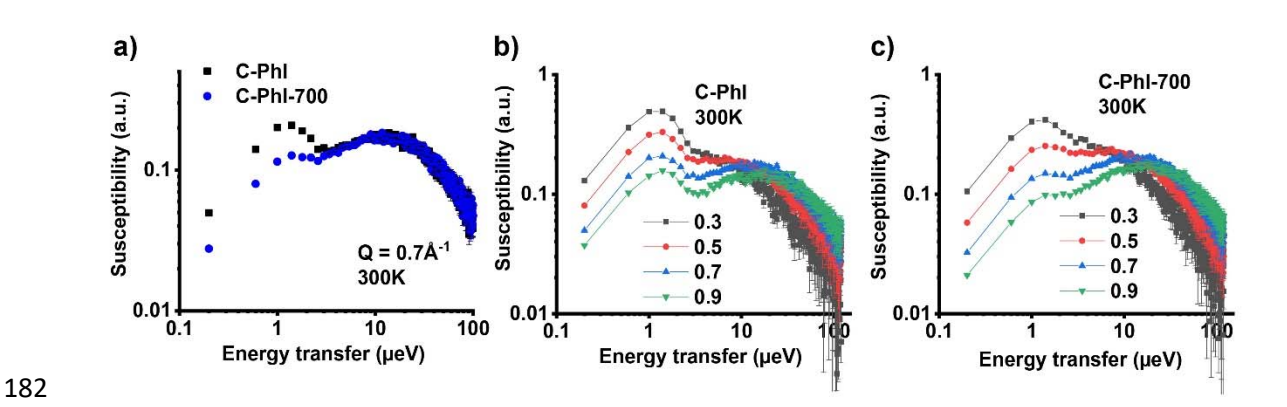


Fig. S6| QENS spectra collected at 300K presented as (a) the dynamic susceptibilities. The data at  $Q = 0.7 \text{ Å}^{-1}$  are shown as representative examples of the behavior of the sample. In (b) and (c), the dynamic susceptibilities are presented at different Q-values.

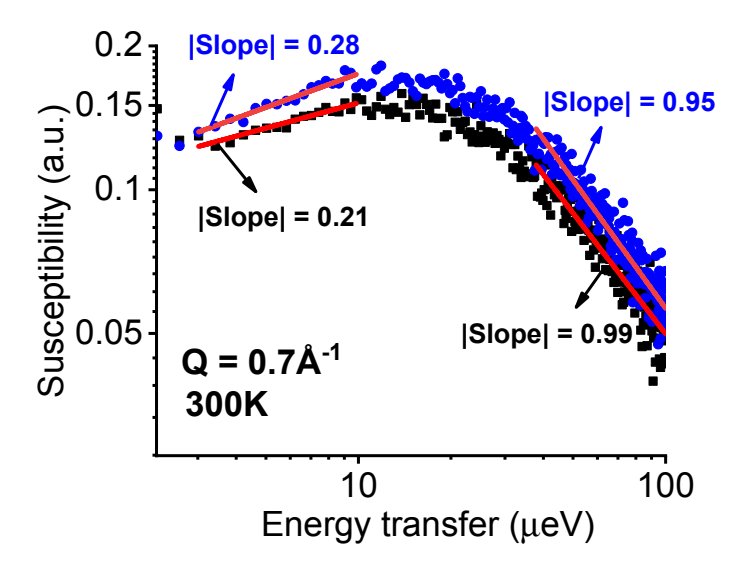


Fig. S7| The relaxations above 10  $\mu eV$  previously shown in Figure S6a are reproduced with the slopes of the low and high-frequency sides being depicted.

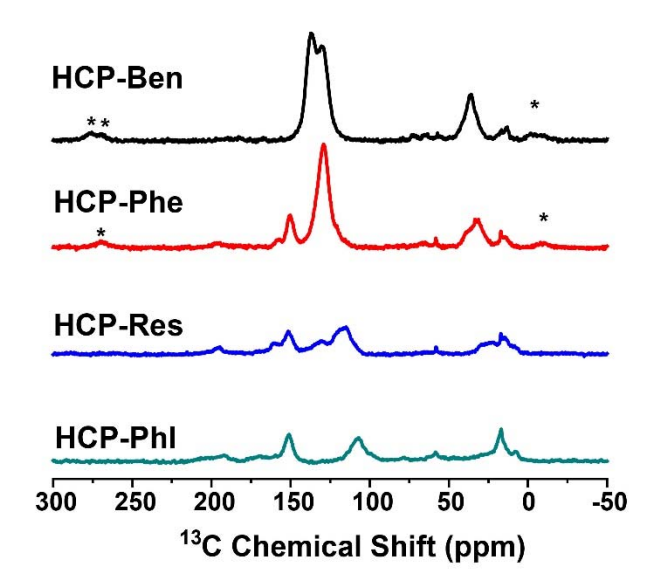


Fig. S8| <sup>13</sup>C CP/MAS NMR of HCPs.

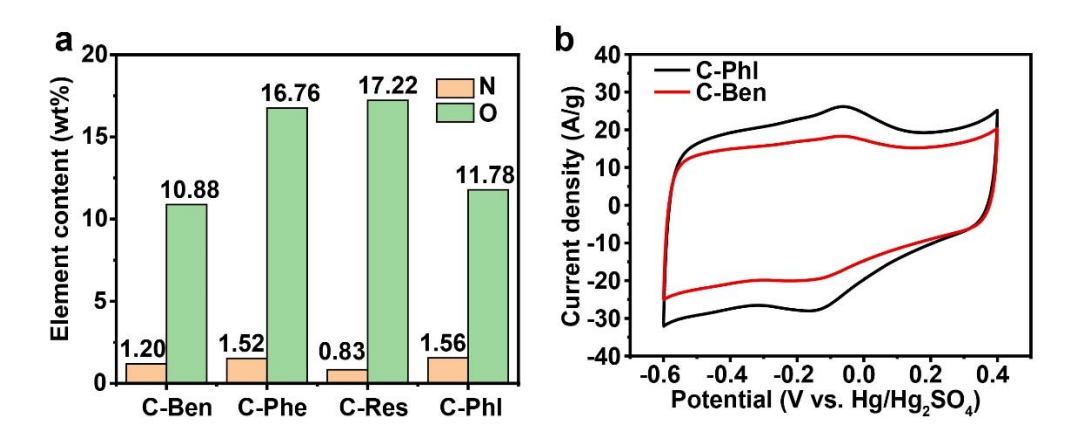


Fig. S9| N and O contents in hyperporous carbons (a) and CV curves of C-Phl and C-Ben at 50 mV/s (b).